Separation and Purification Technology 382 (2026) 135773

Contents lists available at ScienceDirect

Separation and Purification Technology

journal homepage: www.elsevier.com/locate/seppur

Synergistic decontamination of hexavalent chromium and organic pollutants via dual-functional carbon monolith: Deciphering Electrosorption-Electroreduction interplay

Jiangnan Huang [a,b,1], Biao Wang [b,1], Hao-Fan Wang [b], Hongjuan Wang [b], Hao Yu [b], Yonghai Cao [b,*]

[a] College of Chemistry and Chemical Engineering, Zhongkai University of Agriculture and Engineering, Guangzhou 510550, China
[b] School of Chemistry and Chemical Engineering, Guangdong Provincial Key Lab of Green Chemical Product Technology, South China University of Technology, Guangzhou 510641, China

ARTICLE INFO

Editor: Prof. G. Chen

Keywords:
Decontamination
Hexavalent chromium
Organic pollutants
Carbon monolith
Electroreduction

ABSTRACT

The purification of wastewater contaminated with hexavalent chromium (Cr(VI)) and organic pollutants is a pivotal challenge in environmental management. Here, carbon monolith as a catalyst incorporated with a self-designed three-chamber device was developed to shift the Cr(VI) treatment process from the electroadsorption to the electroreduction, which offered 100 % removal efficiency and the ratio of reduction/adsorption (RRA) about 0.92 under an applied voltage of 10 V with a pH of 1. The addition of organic pollutants (MB and PN) into the system facilitated the oxidation process at anode, thereby enhancing the Cr(VI) electroreduction process (as high as 84.4 %), even though the pH value increased to 3 with an applied voltage of 2 V. The value of RRA was enhanced to 1.0 with the low specific energy consumption (5.4 and 7.0 Wh/mol, respectively) and considerable current efficiency (29.6 % and 22.8 %, respectively). Mechanistic insights revealed an interplay between the reactions occurring with this dual-functional carbon monolith for the Cr(VI) electroreduction at the cathode, whereas organic pollutant degradation at the anode, which benefited the removal efficiency and cycling stability.

1. Introduction

The remediation of chromium-containing wastewater stands as a pivotal concern within the environmental restoration [1–3]. Among the various chromium species, Cr(VI) displayed the harmful property due to their extreme toxicity and remarkable propensity for dispersion in aqueous environments [4,5]. The permissible concentration of chromium ion in drinking water is stringently regulated at 0.1 mg/L from the US Food and Drug Administration [3,6]. To mitigate Cr(VI) contamination, treatment strategies typically encompass extraction techniques like adsorption and ion exchange [7–10], alongside electroreduction processes that transform Cr(VI) into the less toxic Cr(III) ions, including photocatalytic and electroreduction pathways [11–13]. However, the limitations of these traditional technology greatly hindered their applications. For the adsorption technology, the properties of the slow kinetics, high cost, complex preparation, and disposal issue of the spent adsorbents were the key limitations [14,15]. Meanwhile, the properties of the fast charge-recombination, low quantum yield, limited light harvesting, and interference by water matrix could be observed in the photocatalysis process [16]. In recent times, electrically propelled adsorption or electroreduction methodologies have emerged with promising advantages, offering low energy consumption and high efficiency in the extraction or treatment of Cr(VI) [17–19]. For instance, an efficient electro-adsorption process with migrating electric-field (0.5 V) aided electrocoagulation was developed, disposing of an effluent of 0.05 ± 0.007 mg/L with low specific energy consumption [20]. Meanwhile, the presence of an electric-field (0.5 V) would significantly increase the adsorption capacity of carbon adsorbent (126.6 mg g^{-1}) [5]. Simultaneously, Cr(VI) could be reduced to Cr(III) ions at −1.2 V, where MOF/Ni foam was used as the working electrode [21]. Also, the modified carbon fiber felt as electrode was found to enhance the electroreduction of Cr(VI) with >0.7 V applied voltage [22]. These work underscore the versatility of electrically driven systems, which can be tailored to yield either electroadsorption or electroreduction outcomes based on

* Corresponding author.
E-mail address: meyhcao@scut.edu.cn (Y. Cao).
[1] These authors contributed equally

https://doi.org/10.1016/j.seppur.2025.135773
Received 24 May 2025; Received in revised form 17 October 2025; Accepted 19 October 2025
Available online 24 October 2025
1383-5866/© 2025 Elsevier B.V. All rights are reserved, including those for text and data mining, AI training, and similar technologies.

operational adjustments across a similar applied potential.

Electroadsorption and electroreduction are inherently dissimilar processes. Electroadsorption operates independently of redox reactions mediated by electron transfer, whereas electroreduction relies on the infusion of external electrons to drive the electrochemical electroreduction of metal ions at the electrode, necessitating a comprehensive evaluation of redox efficiency. Notably, in many electroadsorption configurations, the applied voltage or potential into the system surpasses that required for electroreduction, yet the potential involvement of the electroreduction in these processes also influenced the electrosorption [23–26]. For instance, biocarbon as the adsorbent for the electroadsorption of U(VI) with an applied voltage at 0.4 V ~ 1.2 V was reported, displaying an considerable electrosorption efficiency as high as 94.45 % [23]. Meanwhile, the oxygen electroreduction occurred at the cathode. In fact, the surface –OH groups on carbon would benefit the adsorption/electroreduction of Cr(VI), which could be improved with an applied voltage (0.6 V), and the ratio of reduction/adsorption (RRA) process could be adjusted [24]. Moreover, a multitude of variables, including electrode composition, inter-electrode spacing, electrolyte choice, and voltage intensity, exert influence over both electroadsorption and electroreduction dynamics [27–33].

Electrode material selection also plays a pivotal role in electroadsorption/electroreduction performance [1,13]. Utilizing three-dimensional (3D) carbon materials as electrodes circumvents the activity loss and substrate dilution issues associated with binder requirements in powdered materials [5,34]. In this process, the carbon monolith combined with the through-flow operation was conducive to enhancing the interaction between metal ions and the electrode material, thereby effectively improving the reaction activity [5,24,35,36]. For example, 3D graphene aerogel for the Cu(II) ions adsorption was observed, showing a high efficiency of 1.21 L g_{GA}^{-1} h^{-1} [35]. Our prior investigations demonstrated that 3D carbon monolith materials (MCM) could be applied for the uptake of Cr(VI) and Cu(II) ions with the aid of an electric field [5,36], displaying a considerable Cr(VI) adsorption capacity of as high as 126.6 mg g^{-1}, much higher than that without an electric field (49.5 mg g^{-1}). During that process, no reduction reaction of Cr(VI) to Cr(III) ions was observed [5]. Furthermore, prior research has elucidated the significant impact of electrode thickness on electric field distribution within carbon materials, thereby influencing adsorption efficiency. The reducing carbon material thickness and optimizing electrode spacing not only enhanced adsorption capacity for Pt(VI) ions but also fostered the electroreduction of trace metal ions [37]. Also, the efficient removal of Cr(VI) under both direct current (DC) and alternating current (AC) conditions using the thin electrode materials (5 mm) could be achieved [18,22,38]. Moreover, the carbon monolith materials could afford the well in-situ regeneration ability [5,36,37]. Inspired by these findings, we posit that tailoring the structural attributes (surface characteristics and thickness) of carbon electrode materials, in conjunction with electrode spacing adjustments, can facilitate the transition from electroadsorption to electrochemical reactions.

Herein, in the current study, we engineered and constructed a three-chamber device by minimizing electrode spacing and reducing the thickness of carbon electrodes for the treatment of Cr(VI)-contaminated wastewater. Leveraging MCM and oxidized o-MCM as working electrodes, we successfully orchestrated the transition from electroadsorption to electroreduction of Cr(VI) by modulating the number of carbon electrodes. By doing this, two advantages of this method could be achived: (i) a carbon monolith with a tailed thick (~3 cm) as the electrode benefits the interactions between Cr(VI) and carbon materials. In this process, the solution was forced to flow through the carbon materials and the mass transfer was enhanced. Therefore, the activity of electroadsorption or electroreduction of Cr(VI) could be enhanced. (ii) The well interactions between the Cr(VI) and carbon material would lower the specific energy consumption and increase the ratio of reduction/adsorption in this process. Through an examination of parameters such as pH, initial pollutant concentration, constant potential magnitude, and solution flow rate, we scrutinized the efficiency of electroreduction and its contribution to Cr(VI) removal. Recognizing the interconnected nature of redox reactions, we sought to enhance cathode electroreduction efficiency by augmenting anode oxidation performance. Industrial effluents simultaneously harboring Cr(VI), MB, and PN are most notably in textile dyeing, printing, and leather-tanning operations [16]. No universal "silver bullet" exists for these composite wastewaters: Cr(VI) is a redox-labile heavy-metal oxyanion best handled by reduction to Cr(III) followed by precipitation; MB is a bulky organic dye amenable to adsorptive or oxidative decolorization; PN is a low-molecular-weight micropollutant targeted through biodegradation or advanced oxidation. The divergent removal pathways can mutually interfere, underscoring the need for site-specific, customized treatment strategies. To this end, we introduced prototypical organic pollutants (i.e., methylene blue (MB) and phenol (PN)) as anode oxidation substrates to amplify anode reactions, thereby elevating the electroreduction efficiency and RRA for Cr(VI), while concurrently elucidating the electroreduction mechanism of Cr(VI) within this hybrid system.

2. Experimental section

2.1. Synthesis of three-dimensional carbon catalysts

The three-dimensional carbon materials could be prepared according to our previous work [5,36]. Initially, 45 g of resorcinol and 18.75 g of Pluronic® F127 (block polyether) were dissolved in a binary solvent system comprising 152 mL of absolute ethanol and 120 mL of deionized water with vigorous stirring at 25 °C. Subsequently, 1.56 g of 1,6-hexanediol and 1.16 g of hexamethylenediamine were introduced into the reaction mixture. After 10 min, 61.5 mL of a formaldehyde solution was rapidly incorporated into the stirred mixture, and the system was agitated for an additional 20 min. After that, the obtained emulsion was then transferred to an oven and subjected to a staged thermal treatment: initial curing at 50 °C for 24 h to stabilize the structure, followed by further consolidation at 70 °C for another 24 h, culminating in a high-temperature treatment at 100 °C for 12 h. The obtained solid was then annealed under an inert argon (Ar) atmosphere with a rate of 2 °C/min to temperatures of 900 °C, maintaining for 2 h. The obtained mesoporous carbon material could be denoted as MCM. To enhance the hydrophilicity of the resulting MCMs, a post-treatment was conducted. The MCM samples were immersed in 100 mL of a 3 wt% (H_2O_2) solution and subjected to ultrasonic immersion for 60 min. The obtained carbon catalyst could be denoted as o-MCM.

2.2. Cr(VI) treatment

In this study, we utilized a self-designed three-chamber electrochemical device (each chamber measuring R10 mm × 3 mm with a 5 mm space between them, as illustrated in **Fig. 1a** and **b**) for the remediation of Cr(VI) ion solutions. In this work, we found that the electrode spacing of 5 mm would afford the best activity (**Fig. S1**). In each distinct experiment, a potassium dichromate solution of a predetermined concentration was employed as the contaminant, with o-MCM/MCM acting as the electrode material for both the working and counter electrodes. Under controlled conditions, 400 mL of the potassium dichromate solution was circulated through the carbon electrodes at a specified flow rate using a peristaltic pump. The conditions and their impacts are detailed in the document of Supporting Information. The concentrations of Cr(VI), total chromium ions were measured using UV spectrophotometry (UV–vis, UV-2450) and flame atomic absorption spectrophotometry (AAS, HITACHI Z-2000), respectively.

For the investigation of the synergistic degradation of organic compounds, mixed solutions were prepared by incorporating MB or PN into potassium dichromate solutions. o-MCM was utilized as the electrode material for both the working and counter electrodes. Under continuous stirring, 400 mL of the mixed solution was circulated through the

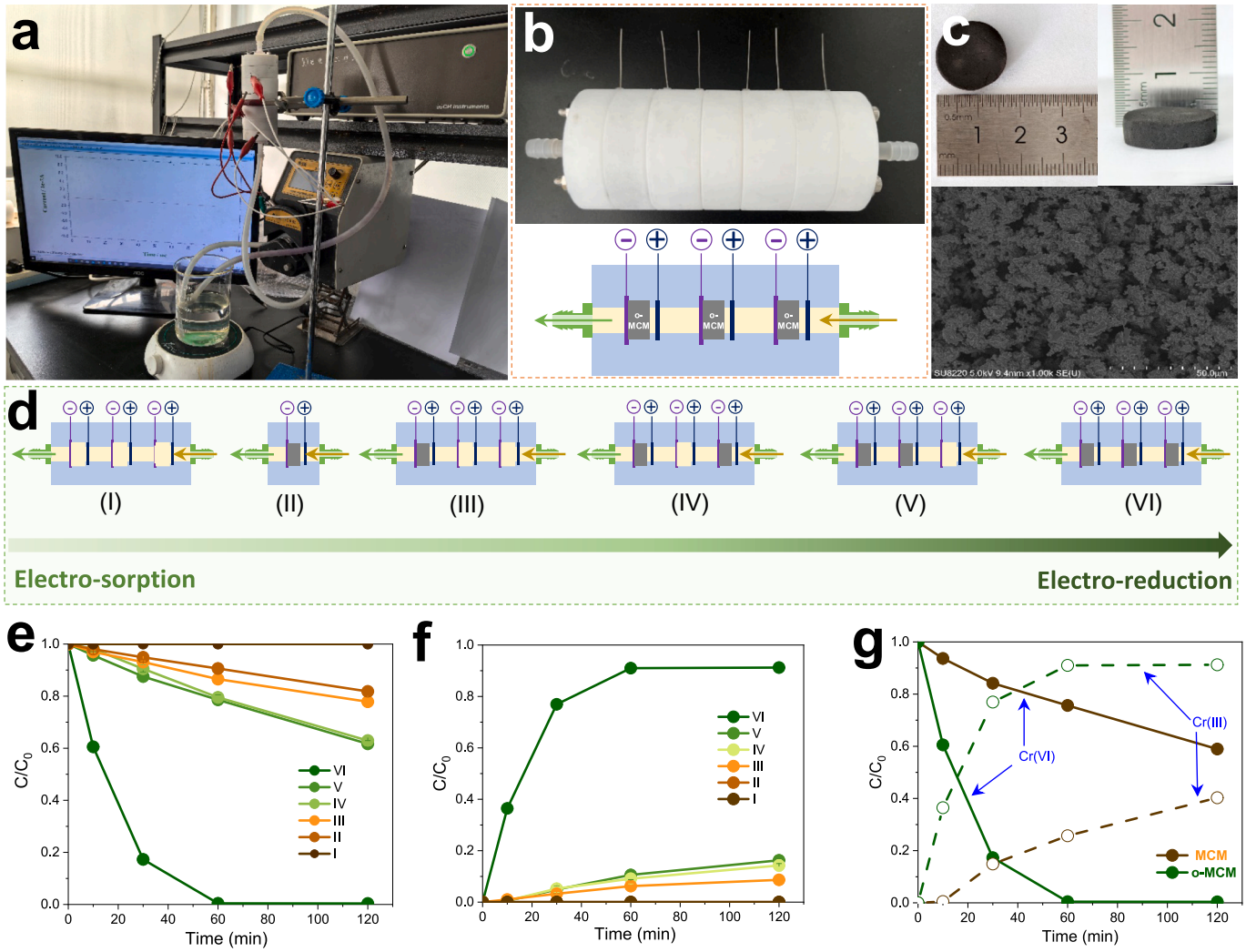

Fig. 1. (a and b) Optical photograph of the self-designed equipment. (c) Optical photo and SEM image of o-MCM. (d) Various settings of the device from electro-sorption to electroreduction. The Cr(VI) removal performance (e) and the generation of Cr(III) ions (f) over different settings. (g) The comparison of MCM and o-MCM in the Cr(VI) removal.

electrodes via a peristaltic pump. The conditions and their impacts are detailed in the file of Supporting Information. In this process, we have evaluated the activity with the presence of Na_2SO_4 under different concentrations (0–10 g/L) (**Fig. S2**). The results demonstrated that the presence of Na_2SO_4 could not affect the activity during the synergistic degradation process. The concentrations of MB, PN, and Cr(VI) were determined using an ultraviolet-visible spectrophotometer (UV–vis, UV-2450), while the concentration of total Cr ions was determined through flame atomic absorption spectrophotometry (AAS, HITACHI Z-2000). The concentration of organic pollutants in the sample solution was determined using the SHIMADZU LC-16 series liquid chromatograph as well. The absorbance values of MB solution at 667 nm and PN solution at 275 nm were detected. Test conditions: temperature 35.0 ± 0.1 °C, total flow rate of mobile phase was 0.500 mL/min, mobile phase methanol + water was (80:20, *V*/V), and injection volume was 10 μL. In this process, the analysis results based on the UV–vis and high performance liquid chromatography (HPLC) were obtained (**Fig. S3**), and we found that no significant disparity between those analysis technology, indicating that the reliable quantification analysis of MB and PN in this work could be achieved. Meanwhile, the value of RRA during the treatment of Cr(VI) could be calculated with **Eq. 1**:

$$RRA = \frac{C_{\triangle Cr(III)}}{C_{\triangle Cr(VI)}} \tag{1}$$

Where $\triangle Cr(III)$ was the concentration of Cr(III) at the eluent, $\triangle Cr(IV)$ was the treated amount of Cr(VI) during the treatment process.

The specific energy consumption (SEC, Wh/mol) and current efficiency (CE) were calculated using the **Eqs. 2–3**:

$$SEC = \frac{USM}{V\Delta c} \tag{2}$$

$$CE = \frac{nV\Delta cN_A}{MS^*1C} \tag{3}$$

Where U, S, M, V, n, and N_A were represented as the applied voltage (V), the total current (A*s), the molar mass of chromium (52 g/mol), the volume of the solution (m^3), the number of electron for the electro-reduction of each Cr(VI) ion ($n = 3$), and Avogadro's constant (6.022×10^{23}), respectively. Δc was the variation of the Cr(VI) ion concentration. 1C (coulomb) was the number of electrons equivalent to 1 A*s ($\sim 6.24 \times 10^{18}$).

3. Results and discussions

3.1. Device and performance

In this study, we successfully synthesized a cylindrical carbon monolith material with three dimensions of R10 mm × 3 mm using PN

and formaldehyde as raw materials through a combined process of thermal polymerization and pyrolysis (Fig. 1**c**). Scanning electron microscopy (SEM) images revealed a complex internal pore structure consisting of both micropores and mesopores (**Fig. S5a**), along with a high specific surface area (SSA) of 686.5 m^2/g, providing a number of active sites for various reactions (**Table S1**). Based on previous research, o-MCM has been identified as an efficient electroadsorbent for Cr(VI) removal when aided by an electric field using our custom-designed equipment [5]. To further enhance the Cr(VI) removal performance, we developed an device featuring a tailored three-chamber structure for treating Cr(VI). This device is characterized by the following notable features: (1) A substantially reduced electrode spacing (from 25 mm to 8 mm), leading to a marked improvement in electron conduction efficiency; (2) A decreased thickness of the MCM (from 20 mm to 3 mm), resulting in a more uniform electric field distribution and enhanced Cr (VI) ion removal efficiency.

Here, we systematically investigated the Cr(VI) removal performance under different device configurations (Fig. 1**d-f**). In the absence of carbon electrodes and with an applied voltage of 10 V, no Cr(VI) removal activity was observed (Device I). The introduction of a single piece of carbon material significantly increased the Cr(VI) removal rate (Device II), achieving adsorption performance comparable to that of the older single-chamber device [5]. Notably, when using Device III, which incorporates a single piece of carbon monolith in a new three-chamber configuration, we not only effectively removed Cr(VI) but also partially converted it to Cr(III), a feat not achievable by the older device, which solely adsorbed Cr(VI). This difference can be attributed to the reduced electrode spacing, which enhanced electron conduction efficiency and accelerated the Cr(VI) electroreduction process. When two pieces of carbon monolith were added to the new device (Devices IV and V), whether arranged consecutively or intermittently, the Cr(VI) removal efficiency was comparable and slightly increased compared to that of Device III. Furthermore, when the number of carbon monoliths was increased to three (Devices VI), as high as 100% of Cr(VI) ion was removed within 60 min, with approximately 90 % of the Cr(VI) being transformed to Cr(III) ions. Moreover, quantitative analyses of SEC and CE were conducted for devices I through VI (**Fig. S4**). Device I exhibited no measurable SEC or CE in this process. In contrast, device II yielded an SEC of 12.81 Wh/mol with a CE of approximately 0 %, which can be attributed to the sole adsorption process. Device III achieved an SEC of about 195.47 Wh/mol with a CE of 14.81 %. Devices IV and V showed comparable performance, with SEC values of 116.91 Wh/mol and 113.08 Wh/mol, and CE values of 24.76 % and 25.60 %, respectively. Notably, device VI demonstrated the lowest SEC (86.99 Wh/mol) and the highest CE (33.27 %) among all devices in this study. Herein, by carefully adjusting the device structure and the amount of carbon material, we successfully transitioned the Cr(VI) treatment process from electroadsorption to electroreduction, thereby introducing a novel technical approach for Cr(VI) remediation. Additionally, the significant disparity in Cr(VI) removal and reduction efficiency between those device might be resulted from the different residence time and the interactions between Cr(VI) and carbon adsorbent in the device.

The surface oxygen-containing groups were believed to benefit the electroadsorption capability for the metal ions [5,36,37,39]. Here, to further reveal the role of surface functionality on the electroreduction of Cr(VI) in this process, MCM without surface modification was used (**Fig. S5b** and **S6**). SEM images and Raman results demonstrated that there is no significant difference between MCM and o-MCM, indicating that they had a similar carbon skeleton. Fourier transform infrared spectrometer (FTIR) analysis displayed that two peaks were located at 3478 cm^{-1} (–OH groups) and 1648 cm^{-1} (–C=O), and more oxygen-containing groups on the o-MCM surface was observed, which would greatly improve the surface hydrophilicity [5,37]. The electroreduction performance over both carbon materials was conducted (Fig. 1 **g**), in which the comparable low activity of MCM was observed. Meanwhile, the much higher concentration of Cr(III) ions over o-MCM than that of MCM was obtained, suggesting that the presence of surface oxygen-containing groups would greatly enhance the electroreduction of Cr (VI) in this process.

To further investigate the surface chemistry of the carbon materials, we performed electrochemical characterization to evaluate the differences in oxygen-containing functional groups (**Fig. S7**). Cyclic voltammetry (CV) results demonstrated notable alterations in the electrochemical behavior after oxidative treatment (o-MCM) (**Fig. S7a**). These changes were primarily characterized by a substantial increase in current density and the emergence of well-defined redox peaks. The CV curve of the pristine MCM exhibited a small enclosed area and a low current response, consistent with typical electric double-layer capacitive behavior. This suggests that the untreated material possesses limited electrochemically active oxygen functional groups on its surface. In contrast, the o-MCM sample showed a dramatically enlarged CV area and significantly enhanced current response. The curve shape deviated from an ideal rectangular form, displaying prominent broad peaks around 0.19 V and 0.74 V. These features indicate the introduction of substantial pseudocapacitance alongside the intrinsic double-layer capacitance, confirming the successful grafting of numerous electrochemically active oxygen-containing groups onto the carbon surface through oxidative treatment. Moreover, the oxidative process not only increased the overall quantity of functional groups but also likely modified their distribution. The enhanced currents at approximately 0.19 V and 0.74 V correspond to the redox activities of quinone/hydroquinone-like and carboxyl/lactone-like species, respectively. The more pronounced current increase in the higher potential region (~0.74 V) implies a preferential formation of acidic oxygen-containing groups, such as carboxyl functionalities, under the given oxidation conditions. Additionally, the oxidative treatment improved surface hydrophilicity and ion accessibility, promoting electrolyte wetting and penetration. This enhanced interfacial property represented another critical factor contributing to the superior capacitance of o-MCM, as it enabled more efficient utilization of the available surface area, including internal pore structures, for electrochemical charge storage.

The surface properties of carbon materials may cause electrode polarization, leading to energy loss (**Fig. S7b**). After oxidation treatment with hydrogen peroxide, the increased reductive functional groups on the surface of carbon materials, such as hydroxyl and carboxyl groups, may undergo oxidation reactions at high potentials. In this study, hydroxyl groups were oxidized to carbonyl groups, and carboxyl groups may further undergo decarboxylation reactions. These oxidation processes corresponded to the slight increase in current density at high potentials in the curve. The introduced oxygen-containing functional groups provided more electrochemical active sites for the carbon materials, enabling more efficient catalytic reduction reactions at low potentials, which explained the larger reduction current in the low-potential region of the curve. The LSV and CV curves were tested at the same scan rate, and in the experimental results, the LSV curve corresponded to the oxidation segment of the CV curve. The CV curve shows that the peak potential difference ΔE_p for the oxidation-reduction reaction on the MCM electrode surface was 0.55 V, which deviated from the corresponding value of 0.057 V for a single-electron transfer reaction at 25 °C [40], indicating the presence of polarization. It is speculated that this polarization phenomenon may be caused by oxygen-containing functional groups such as −OH and − C=O on o-MCM. According to the Eq. 4, the calculated W_{loss} was 5.4×10^{-4} Wh, which was far lower than the current system energy and did not have a direct impact on the system.

$$W_{loss} = \eta \int \Delta I(E) dt \tag{4}$$

Where W_{loss} (Wh) represented the electrode polarization energy loss of a single voltammetric cycle. η represented the overpotential (V). $\Delta I(E)$ (A) in the CV curve was defined as the difference between the oxidation-reduction peak current and the dashed line current, taken as a positive

value. *t* represented time (*h*).

The influence of various parameters on the electroreduction of Cr(VI) within our device was meticulously examined (Fig. 2). Voltage, defined as the potential difference applied between the two electrodes during the electroreduction process, is a critical factor in the electroreduction process. Typically, a higher applied voltage introduces more energy into the electroreduction process, thereby promoting the electroreduction of Cr(VI). Currently, when the applied voltage was set to 0 V (i.e., open-circuit voltage), a slight activity for the Cr(VI) removal was observed, without generating Cr(III) ions, indicating the sole adsorption process of Cr(VI). When the applied voltage was increased to 2 V, the removal of Cr (VI) was notably enhanced, and RRA also rose accordingly. As the applied voltage continued to rise to 10 V, the electroreduction reaction of Cr(VI) accelerated, and the concentration of Cr(III) ions increased significantly, leading to a substantial improvement in the electroreduction ratio (RRA > 0.9). This result demonstrated that increasing the voltage can effectively enhance electron transfer and the rate of the electroreduction reaction in the electrochemical system, thereby significantly boosting the electroreduction process. Overall, the RRA value increased from 0 to 0.92 with an increase in the applied voltage (0–10 V). Based on the reported literature, it was understood that Cr(VI) may receive electrons at the cathode and undergo the electroreduction reaction described by the **Eq.** 4. However, when the applied voltage exceeded 6 V, a significant amount of bubbles formed, attributed to enhanced Faraday side reactions (i.e., water electrolysis), which caused the electroreduction efficiency to plateau (RRA < 1).

$$Cr_2O_7^{2-} + 6e^- + 14H^+ \rightarrow 2Cr^{3+} + 7H_2O \quad (4)$$

pH value is a significant parameter for the Cr(VI) removal, and the electroreduction of Cr(VI) is usually carried out under acidic conditions

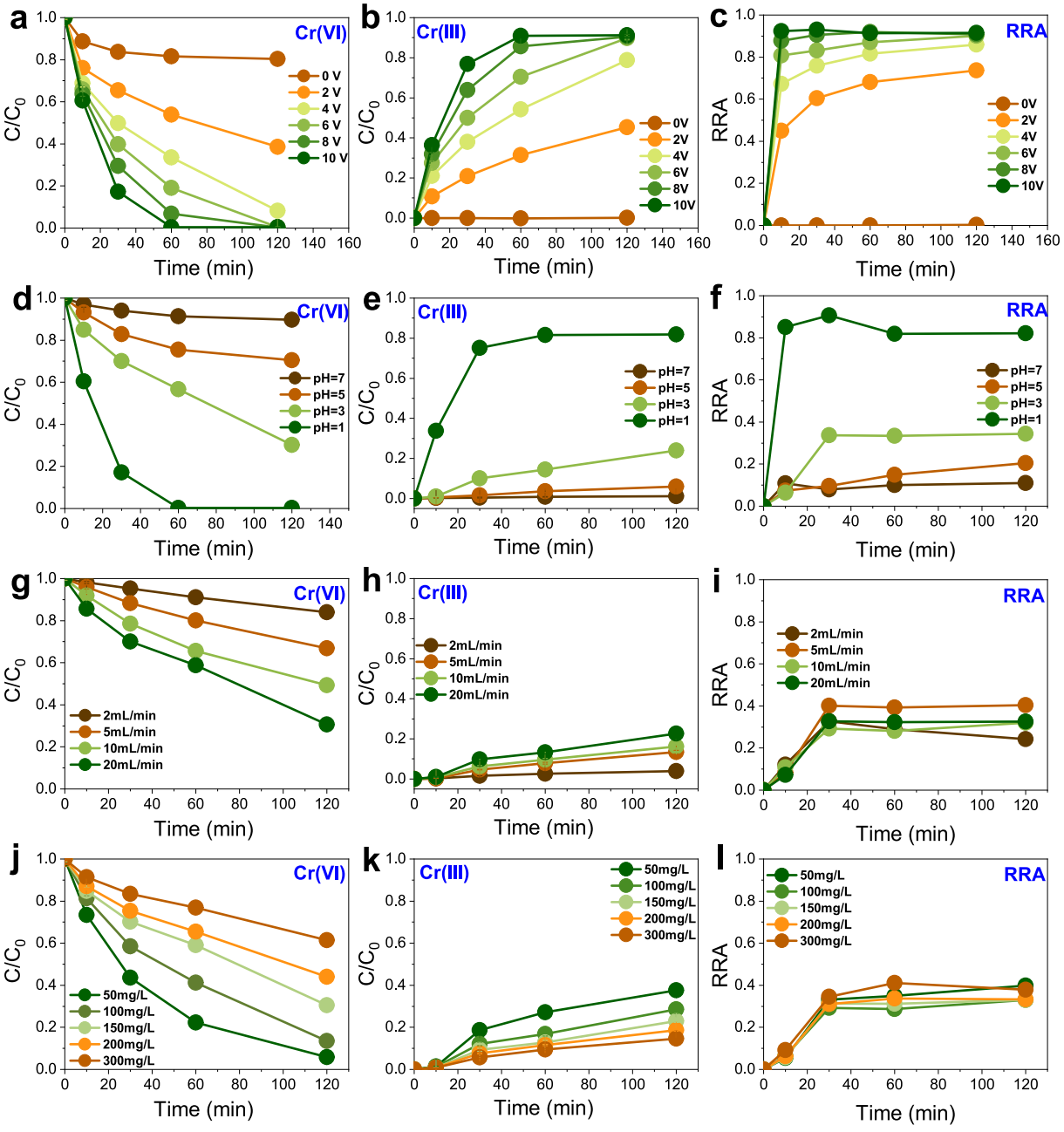

Fig. 2. Effect of different parameters such as applied voltage (a-c), pH value (d-f), flow rate (g-i), initial Cr(VI) concentration (j-l) on the Cr(VI) removal, Cr(III) generation, and RRA, respectively.

due to the higher redox potential and oxidability of Cr(VI) [41]. Generally, the wastewater containing Cr(VI) in industry is acidic. Herein, the pH value could be adjusted to 1, 3, 5, and 7, respectively. When the initial pH value was 7, only 10 % of Cr(VI) were removed with a low RRA (~0.10) within 120 min. Furthermore, when the initial pH value was lowered to 3 and 5, the removal rates increased to 30 % and 70 %, respectively, while, RRA of both increased to 0.20 and 0.34, respectively. When the initial pH value was further lowered to 1, the concentration of Cr(VI) decreased sharply within 60 min, at which point most of the Cr(VI) were converted to Cr(III) ions with the RRA maintained between 0.8–0.9. In this process, the low pH value with a high concentration of H^+ in the system was conducive to the electroreduction of Cr(VI) [10,42].

The flow rate of the solution determines the amount of Cr(VI) that flow through the electrode surface per unit operation time. In this work, as the flow rate increased from 2 to 20 mL/min, the removal efficiency of Cr(VI) also significantly improved from 16 % to 69 %. This indicated that a high flow rate could increase the number of times the solution circulates through the electrode, which was favorable to remove more Cr(VI). Meanwhile, the concentration of Cr(III) slightly increased (C/C_0 increased from 0.04 to 0.22) alongside with the increase of flow rate. However, based on the value of RRA for these conditions (fluctuating between 0.24 and 0.40), we could not conclude that the electroreduction process was improved by increasing the flow rate. Therefore, we believe

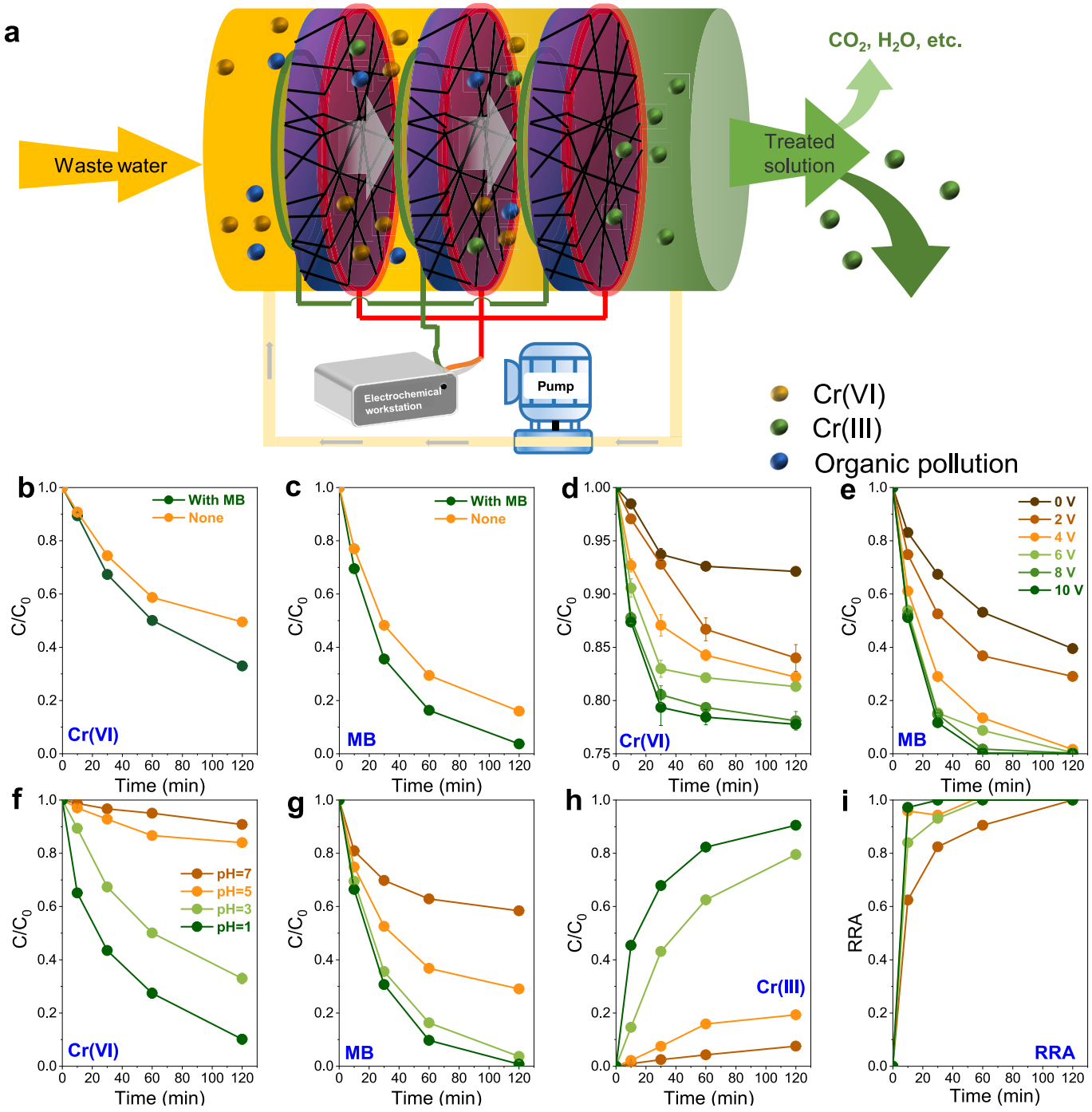

Fig. 3. (a) Schematic illustration of the electroreduction of Cr(VI) with the organic pollution. The Cr(VI) removal (b) and MB degradation (c) with or without the synergistic effect. The effect of applied voltage (d-e) and pH (f-i) on the performance.

that the variation of the flow rate could not apparently change the ratio of electroadsorption/electroreduction. Additionally, the initial concentration of Cr(VI) also affected the electroreduction efficiency. In this experiment, as the initial concentration of Cr(VI) continuously increased from 50 to 300 mg/L, the removal rate of Cr(VI) decreased from 95 % to 39 %, ascribed to the limited number of active sites on the surface of the electrode material, since more electrons were need at the high concentration of Cr(VI). Meanwhile, the concentration of Cr(III) in the solution also showed a corresponding decrease, and the value of RRA fluctuated between 0.33 and 0.40, indicating that changes in concentration do not affect the proportion of electroreduction reactions.

3.2. Synergistic degradation

Based on the principles of electrochemical reactions, Cr(VI) typically undergoes an electroreduction process at the cathode, while oxidation reactions occur at the anode. These reactions at the cathode or anode influence the performance on the other side [43]. Previous studies have shown that when the applied voltage was increased >6 V, a significant number of bubbles were generated in the reaction system due to Faraday side reactions, primarily water electrolysis occurring at the anode. Additionally, Cr(VI) were not totally transformed to Cr(III) ions, and adsorption played a considerable role in the process (**Fig. 1**). Generally, in an electrochemical system, the reactivity at one electrode will affect the efficiency of the other electrode [44]. The high energy with the presence of water electrolysis at the anode lowered the electroreduction efficiency at the cathode.

Herein, the easily oxidizable organic compounds to facilitate the oxidation process at the anode were introduced into the reaction system, thereby improving the electroreduction reaction at the cathode. In this study, we selected two typical water pollutants, MB and PN, as sacrificial agents to boost the electroreduction efficiency at the cathode (Fig. 3a). In fact, the industrial effluents from the textile dyeing, printing, and leather-tanning operations usually contain Cr(VI) and organic pollutants, which needs the site-specific, customized treatment strategies to treat them simultaneously. In current work, we try to added typical organic pollutants such as MB and PN to verify the feasibility of the developed treatment process to remove Cr(VI) and organic pollutants simultaneously. Before the test, we have evaluated the influence of the typical ions on the electroreduction of Cr(VI) in the presence of organic pollutants (**Fig. S8**). The results demonstrated the negligible influence of these ions on the removal efficiency, further indicating that the presence of MB or PN acted as the electrolyte for the process as well, facilitating the electroredution of Cr(VI).

Here, MB as a sacrificial organic substrate was incorporated into the reaction system, in which the Cr(VI) removal performance increased by 1.43-fold, compared to non-synergistic conditions (**Fig. 3b** and **c**). This confirms that introducing organic sacrificial agents can markedly enhance Cr(VI) removal efficiency. We next examined the effect of applied voltage on the synergistic treatment of Cr(VI) and MB (**Fig. 3d** and **e**). As the potential rose, the removal rates of both contaminants improved significantly. At 2.0 V, the removal efficiencies of Cr(VI) and MB were 2.22-fold and 1.58-fold higher, respectively, than those with the absence of an applied voltage at the pH of 5. This suggested that elevating the potential accelerated the short-term removal of Cr(VI) but also accelerated MB degradation at the anode. Notably, the increase in applied voltage could not significantly enhance the activity, probably due to the high pH value. Regarding pH effects (**Fig. 3f** and **i**), the removal efficiency of Cr(VI) increased progressively as the initial solution pH decreased. In contrast, pH had a less pronounced impact on MB degradation compared to Cr(VI) removal. This discrepancy likely arises because Cr(VI) exhibit stronger oxidizing properties at lower pH values, facilitating their electroreduction and thereby reducing reliance on MB as a sacrificial agent. Notably, the concentration of Cr(III) ions rose sharply as the pH fell from 7 to 1. Moreover, when the pH was below 5, the value of RRA approached ~1 even the applied voltage was 2 V, much higher than that of the reaction system without MB (RRA was about 0.7, Fig. 2i), indicating efficient Cr(VI)-to-Cr(III) conversion under acidic conditions. Additionally, no bubble formation was observed during these processes.

PN as a sacrificial agent for anode oxidation was then applied to the reaction system as well (Fig. 4). Under synergistic treatment, the removal performances for the Cr(VI) and PN were 1.33 times and 1.35 times higher, respectively, than those without synergism, demonstrating a good synergistic improvement for the Cr(VI) and PN treatment (Fig. 4a-b). By adjusting the applied voltage, we found that the activity also significantly increased with the increase in voltage (Fig. 4c-d**)**. Especially, when a voltage of 2.0 V was applied, the performances for Cr (VI) and PN were 2.04 times and 3.0 times higher, respectively, than those without voltage at the pH of 5. The influence of pH on this process was further explored (Fig. 4e–h**)**. The results showed that the removal performance for Cr(VI) and PN continuously increased as the pH value of the solution decreased. During this process, the Cr(III) ions were also rapidly generated. Notably, the improvement with the addition of PN was higher than that in the presence of MB, due to the π-π interaction between PN and carbon catalysts [45]. Whereas, the value of RRA in the PN system was lower than that in the MB system, with a maximum value of 0.75 at a pH of 7 (<1). This performance may be resulted from the higher difficulty of PN oxidation compared to MB at the anode, affecting the Cr(VI) electroreduction at the cathode. Meanwhile, it might be argued that the reduction of Cr(VI) would be affected by the coexisting MB/PN in the analytical procedure. In this work, we tested the concentration variations of Cr(VI) with the coexisting MB/PN without treatments (**Fig. S9**). The results demonstrated that both systems with the coexisting MB/PN displayed the low removal efficiencies for Cr(VI), MB, and PN during the analytical procedure, indicating that the electroreduction of Cr(VI) dominate the processes.

The comparison of three reaction systems over the reaction kinetic, SEC and CE were conducted. We found that the pseudo-first-order reaction constant (k) for the electroreduction without organic pollutant (k_{None}) increased from 0.005 to 0.15 h^{-1} with the increase of the applied voltage (0–10 V) (**Fig. 5**a). When PN was added into the reaction system, k_{PN} (0.11–0.36 h^{-1}) was much higher than k_{None} across the whole applied voltage (0–10 V). Furthermore, the addition of MB would significantly enhance the reactivity. k_{MB} was increased from 0.18 to 0.84 h^{-1} along with the increase of the applied voltage. Especially, k_{MB} was 5.6-fold higher than k_{None} under an applied voltage of 10 V. These results confirmed that the addition of organic pollutant (MB or PN) could efficiently enhance the kinetic activity. Meanwhile, the variation of SEC and CE over these reaction systems were observed (**Fig. 5**b and c). Although the increase of the applied voltage could apparently increase SEC and lower CE, the system with MB or PN could still greatly reduce SEC and increase CE, compared to that without the organic pollutant. Notably, SEC_{MB} (21.6–54.0 Wh/mol) was higher than SEC_{PN} (13.9–25.4 Wh/mol) when the applied voltage was >6 V, while, the CE_{PN} (11.6 % ~ 6.3 %) was much lower than CE_{MB} (22.3 % ~ 14.9 %). These results probably ascribed to the easy oxidation of MB at the anode, which would transfer more electrons to Cr(VI) to generate Cr(III) ions.

Herein, we can confirm that the introduction of organic compounds at the anode can effectively improve the Cr(VI) electroreduction to Cr (III) ions at the cathode. Although a comparable low CE was observed (29.6 % for MB, 22.8 % ford PN), the process developed in this study offers the advantages of low energy consumption (5.4–7.0 Wh/mol) and high RRA (~1.0) under a pH value of 3. This energy consumption was much lower than that of titanium plate (659,000 Wh/mol) [46], RVC (436.8 Wh/mol) [47], copper meshes (3867 Wh/mol) [48], and RVC-PANI (369.2 Wh/mol) [49] et al. (**Table S2**), further fulfilling the goals of low cost and environmental friendliness. Therefore, the use of shaped carbon materials for electroreduction and synergistic removal of Cr(VI) and organic compounds holds promising application prospects.

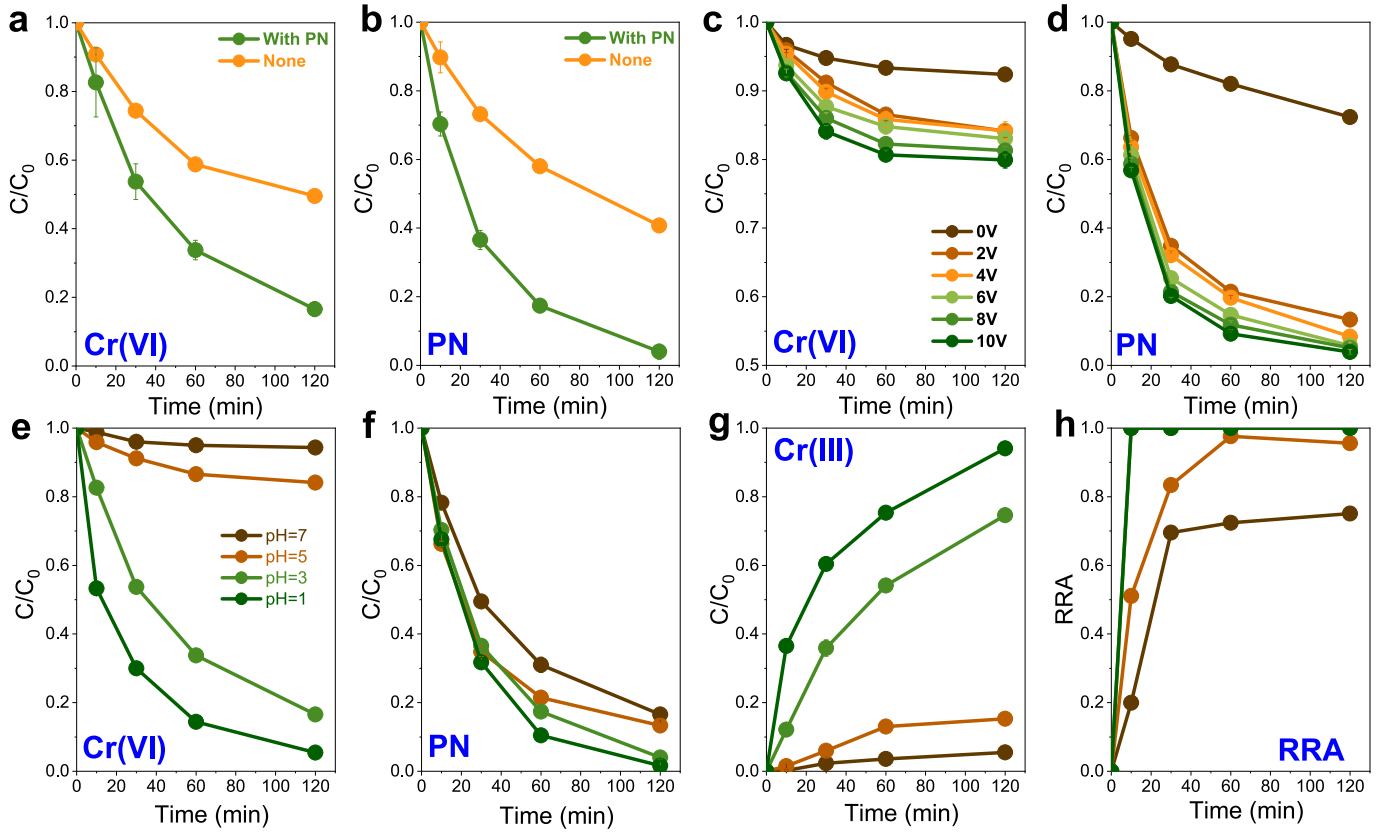

Fig. 4. The comparison of Cr(VI) removal (a) and PN degradation (b) with or without the synergistic effect. The effect of applied voltage (c-d) and pH (e-h) on the performance.

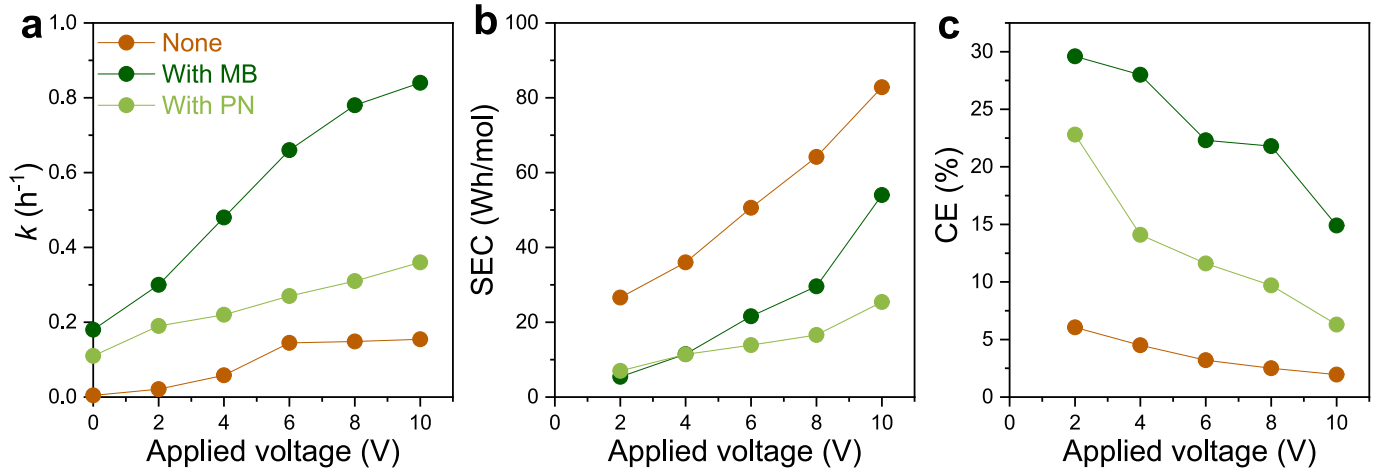

Fig. 5. The pseudo-first-order reaction constant (*k*) (a), SEC (b) and CE (c) of the electroreduction of Cr(VI) ion under different applied voltage.

3.3. Stability test

Stability stands as a pivotal parameter for gauging the efficiency of electroreduction and serves as a fundamental criterion for evaluating the possibility of a technology's industrial applicability. In this study, o-MCM as the catalyst was utilized for the recycle stability of the synergistic catalytic electroreduction and degradation process involving Cr (VI) and organic compounds (Fig. 6). Before the recycling, the used carbon catalyst would be regenerated by applying the reverse voltage (2 V) with hot water (90 °C) to remove the adsorbed substrates or by-products on the surface. The experimental results revealed that during the 6 recycle tests, the activity of carbon catalyst with MB or PN displayed a comparably higher activity than that without organic components in the solution. And the presence of PN was more favorable to enhance the activity. Nevertheless, the activity of these three systems (blank, with MB or PN) exhibited a notable decrease at the initial three recycles, and then the removal performance stabilized at the fourth to sixth recycles. Meanwhile, for the degradation process of MB and PN, the exceptionally high stability was observed as well (**Fig. S10**). It was noteworthy that a slight decline in the removal rate of PN after six cycles, which might stem from the inherent difficulty in the ring-opening of PN molecules.

The comprehensive characterizations for analyzing the surface physical/chemical properties of the used carbon catalyst were

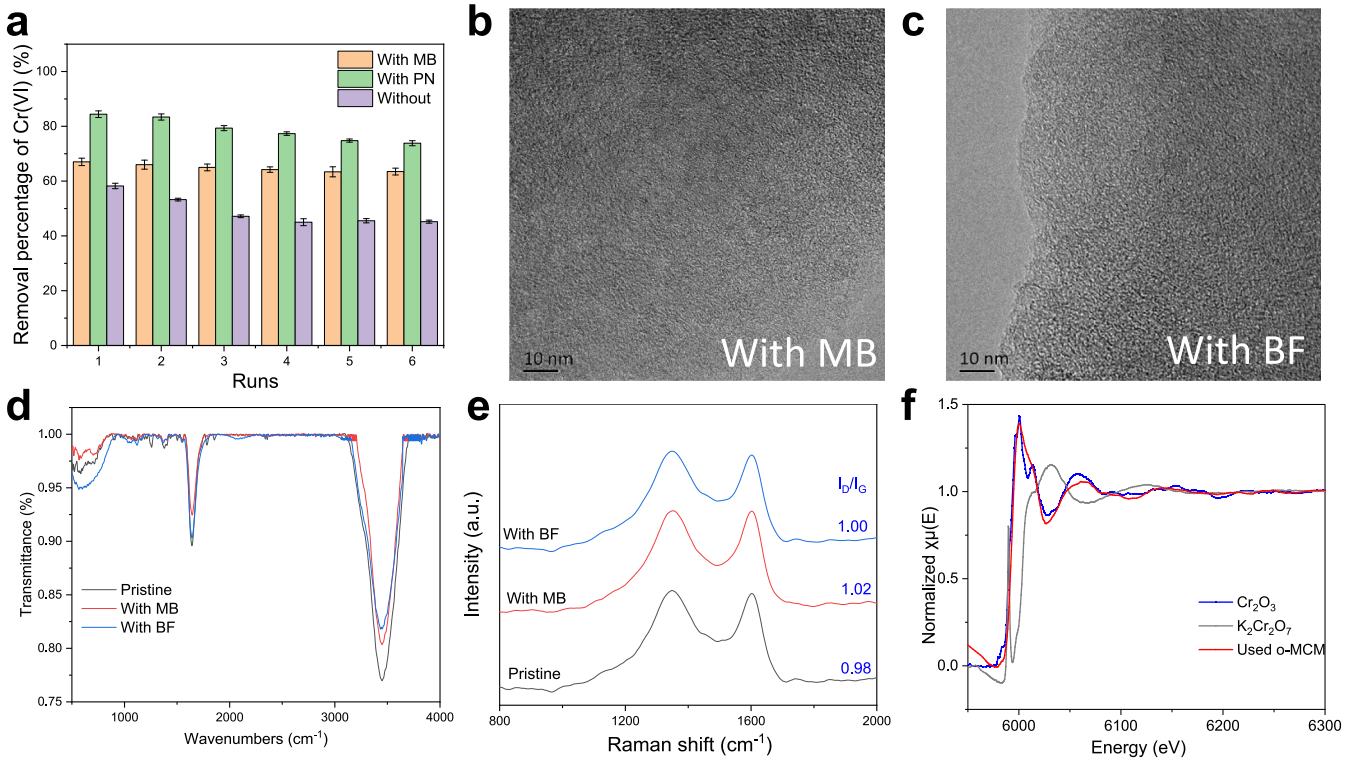

Fig. 6. (a) The cyclic stability of the Cr(VI). The TEM image (b-c), FTIR (d), Raman spectra (e) of the used o-MCM. (f) The XANES analysis of the Cr valence state on the used o-MCM.

conducted (Fig. 6b-f, **S11-S13**). TEM images of the used adsorbent with MB or PN revealed that the porous carbon structure did not change significantly. FTIR results indicated that the material surface functional groups slightly increased, probably ascribed to the oxidation reaction between the Cr(VI) and edge carbons, which were also confirmed by the Raman results (the value of I_D/I_G increased slightly). The XPS results provided compelling evidence that the material surface after the synergistic reaction with MB and PN was predominantly composed of Cr(III) ions, which displayed a low content on the carbon surface. Furthermore, the XANES analysis of the valence state of Cr on the surface of the used o-MCM was conducted. It was found that there was no apparent Cr(VI) on the carbon surface, and only Cr(III) could be observed, confirming the efficient electroreduction of Cr(VI) to Cr(III) during the treatment process via the laboratory-designed device. However, the significant decrease of the specific surface area (SSA) of the used carbon material from 686.5 m^2/g to 337.3 m^2/g in the non-synergistic Cr(VI) electroreduction system was observed (**Table S1**), indicating that a considerable amount of Cr(VI) adsorption occurred and these Cr(VI) blocked the pores inside the carbon monolith adsorbent. While, SSA of the used carbon material with MB or PN decreased moderately (516.8 and 542.1 m^2/g for MB and PN, respectively), suggesting that the Cr ions could be removed from the carbon interface, subsequently making the regeneration of carbon adsorbent to improve the activity.

3.4. Mechanism study

Herein, the synergistic degradation-electroreduction experiment for the simultaneous removal of Cr(VI) and organic pollutants was illustrated (Fig. 7). As for the Cr(VI) electroreduction at the cathode, we have found that the surface oxygen-containing groups on o-MCM would facilitate the activity (**Fig. 1 g**) [5]. Here, we believe that the electroreduction process could be elucidated as four steps (I ~ IV). The surface oxygen-containing groups on o-MCM could act as the key sites for the interaction with Cr(VI). These oxygen-containing groups tightly adsorbed Cr(VI), transferring electrons from the carbon electrode to the Cr (VI), where Cr(III) ions were generated and dispersed into the solution.

On the basis of the aforementioned discussion, the electroreduction of Cr(VI) at the cathode would be greatly influenced by the oxidation process at the anode. Therefore, to gain deeper insights into the degradation mechanism of these organic contaminants, the solutions with the degradation products formed during the degradation process were analyzed. According to the literature, the degradation of MB mainly underwent three steps, including methylation, desulfurization, and ring-opening reactions. The intermediate compounds, such as 5-amino-2-nitrobenzoic acid, 4-aminobenzoate, and 2-benzoxazolone, etc., were easily oxidized into CO_2, H_2O, and other inorganic ions with the assistance of the electrooxidation and the strong oxidizing ions (CrO_4^- and $Cr_2O_7^{2-}$) [50,51]. In this work, the HPLC-MS analysis of the MB solution after reaction was carried out (**Fig. S14**). No apparent intermediate products were detected, indicating that the degradation process of MB was facilitated to produce CO_2 and H_2O. The chemical oxygen demand (COD) analyses revealed that almost 86.0 % MB was mineralized in this process (**Table S3**), further confirming the significant incorporation of MB in the reaction. XPS test results indicated that the Cr element content on the carbon material surface was very low, indirectly suggesting that the adsorption of Cr(VI) by the electrode material is not significant in this system, thereby effectively facilitating the redox reaction.

For the degradation of PN at the anode, the solution with the intermediates and COD value after the electrodegradation experiment was analyzed as well. According to the COD analysis, the COD value of the solution slightly changed after the reaction (18.8 %), suggesting that PN was ultimately challenging to fully degrade into CO_2 and H_2O. based on the reported literature, the degradation process of PN involves two stages: hydroxylation and the opening of the benzene ring conjugate structure [52,53]. The HPLC-MS analysis of the PN solution after reaction was carried out (**Fig. S15**). However, we found that the molecular masses of the detected products all deviated from the normal value range, which might be resulted from the complexation of Cr ions with the intermediate substances. This complexation might be the reason for the comparably low RRA activity (Fig. 4h). Nevertheless, identifying this

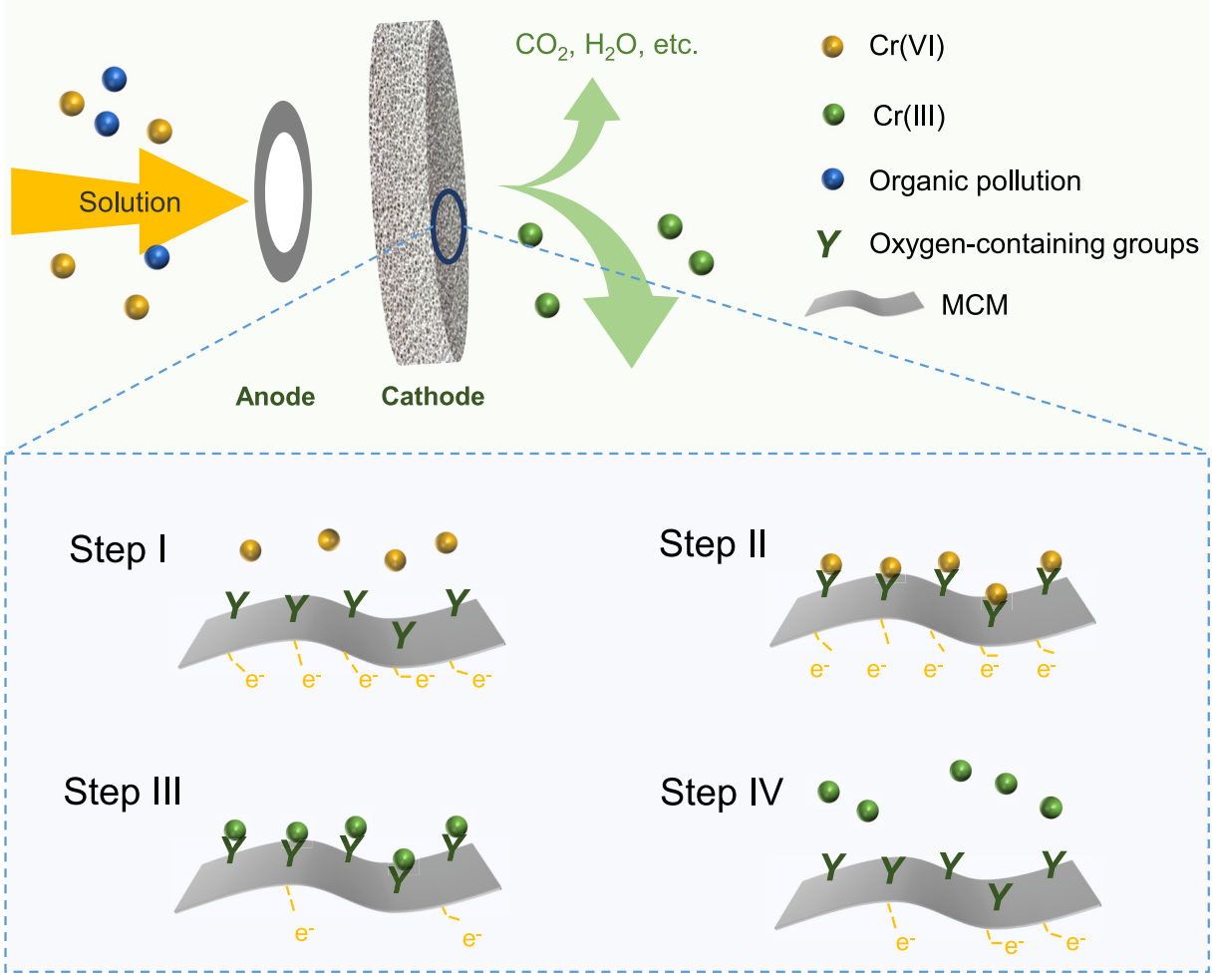

Fig. 7. The schematic illustration of the electroreduction mechanism of Cr(VI) on the surface of o-MCM.

complexation process and degrading the complex compound are very difficult at current stage, which would be thorough investigated in our subsequent work.

4. Conclusions

In summary, a tailored device with three chambers using carbon monolith materials with surface modification as electrodes was developed for the electroreduction of Cr(VI) at the cathode with the oxidation degradation of organic pollutants at the anode. Specifically, without the involvement of organic contaminants, the removal efficiency of Cr(VI) was almost 100 % with an RRA about 0.9 when the pH value of 1 and an applied voltage of 10 V were applied, displaying a high energy consumption (41.4 Wh/mol) and low CE (3.9 %). With the presence of organic contaminants (MB and PN), the greatly enhanced efficiency of Cr(VI) with an improved RRA was about 1.0 when a pH value of 3 and an applied voltage of 2 V were applied. This results ascribed to the lowered difficulty of the oxidation reaction occurring at the anode, thereby increasing the activity of the electroreduction of Cr(VI). By doing this, the energy consumption could be decreased to (5.4 Wh/mol and 7.0 Wh/mol, respectively) and electron efficiency increased to (29.6 % and 22.8 %, respectively). In this process, the surface oxygen-containing groups dominated the Cr(VI) removal efficiency. And the property of being easily oxidized for the organic contaminants at the anode would significantly influence the Cr(VI) electroreduction at the cathode. Here, 86.0 % MB could be mineralized to CO_2 and H_2O, which greatly benefited the electroreduction of Cr(VI). Meanwhile, when PN was used, the removal efficiency of PN was >95 %, but the mineralization of PN was only 18.8 %, which resulted in a comparably low activity in a low Cr (VI) electroreduction efficiency with the presence of PN, compared to that with MB. This work paved a new strategy for the sustainable treatment of wastewater containing Cr(VI) and organic contaminants.

CRediT authorship contribution statement

Jiangnan Huang: Writing – review & editing, Writing – original draft, Resources, Methodology. **Biao Wang:** Writing – original draft, Investigation, Data curation. **Hao-Fan Wang:** Resources, Methodology. **Hongjuan Wang:** Resources, Methodology. **Hao Yu:** Resources, Methodology. **Yonghai Cao:** Writing – review & editing, Supervision, Resources, Project administration, Methodology.

Declaration of competing interest

The authors declare that they have no known competing financial interests or personal relationships that could have appeared to influence the work reported in this paper.

Acknowledgements

We would like to acknowledge the financial support from the National Natural Science Foundation of China (22272056), Guangdong Basic and Applied Basic Research Foundation (2022A1515140108), CNPC Innovation Found (2021DQ02-0704), Research Fund Program of

Guangdong Provincial Key Laboratory of Fuel Cell Technology (FC202305), and the start-up fund from Zhongkai College of Agricultural Engineering.

Appendix A. Supplementary data

Supplementary data to this article can be found online at https://doi.org/10.1016/j.seppur.2025.135773.

Data availability

Data will be made available on request.

References

[1] H. Yin, L. Huang, Y. Dai, Z. Zheng, Y. Li, B. Tang, X. Wang, L. Shi, In-situ redox processes of electrosorption-based systems during as, Cr detoxification and recovery: mechanisms, applications and challenges, Chem. Eng. J. 503 (2025) 157946.

[2] X.-Z. Fu, J. Wu, S. Cui, X.-M. Wang, H.-Q. Liu, R.-L. He, C. Yang, X. Deng, Z.-L. Tan, W.-W. Li, Self-regenerable bio-hybrid with biogenic ferrous sulfide nanoparticles for treating high-concentration chromium-containing wastewater, Water Res. 206 (2021) 117731.

[3] M.S. Bashir, N. Ramzan, T. Najam, G. Abbas, X. Gu, M. Arif, M. Qasim, H. Bashir, S. S.A. Shah, M. Sillanpää, Metallic nanoparticles for catalytic reduction of toxic hexavalent chromium from aqueous medium: a state-of-the-art review, Sci. Total Environ. 829 (2022) 154475.

[4] J. Zhu, S. Wei, H. Gu, S.B. Rapole, Q. Wang, Z. Luo, N. Haldolaarachchige, D. P. Young, Z. Guo, One-pot synthesis of magnetic graphene nanocomposites decorated with Core@double-shell nanoparticles for fast chromium removal, Environ. Sci. Technol. 46 (2012) 977–985.

[5] B. Wang, Q. Jiang, G. Yang, H. Wang, H. Wang, F. Peng, H. Yu, J. Huang, G. Zhong, Y. Cao, Electric field-assisted uptake of hexavalent chromium ions with in situ regeneration of carbon monolith adsorbents, Adv. Sci. 10 (2023) 2301419.

[6] Y. Cao, J. Huang, X. Peng, D. Cao, A. Galaska, S. Qiu, J. Liu, M.A. Khan, D. P. Young, J.E. Ryu, H. Feng, N. Yerra, Z. Guo, Poly(vinylidene fluoride) derived fluorine-doped magnetic carbon nanoadsorbents for enhanced chromium removal, Carbon 115 (2017) 503–514.

[7] Y. Sun, F. Yu, L. Li, J. Ma, Adsorption-reduction synergistic effect for rapid removal of Cr (VI) ions on superelastic NH_2-graphene sponge, Chem. Eng. J. 421 (2021) 129933.

[8] Y. Song, G. Wei, M. Kopeć, L. Rao, Z. Zhang, E. Gottlieb, Z. Wang, R. Yuan, G. Ye, J. Wang, T. Kowalewski, K. Matyjaszewski, Copolymer-templated synthesis of nitrogen-doped mesoporous carbons for enhanced adsorption of hexavalent chromium and uranium, ACS Appl. Nano Mater. 1 (2018) 2536–2543.

[9] J. Xing, C. Zhu, I. Chowdhury, Y. Tian, D. Du, Y. Lin, Electrically switched ion exchange based on Polypyrrole and carbon nanotube nanocomposite for the removal of chromium(VI) from aqueous solution, Ind. Eng. Chem. Res. 57 (2018) 768–774.

[10] J. Huang, Y. Li, Y. Cao, F. Peng, Y. Cao, Q. Shao, H. Liu, Z. Guo, Hexavalent chromium removal over magnetic carbon nanoadsorbents: synergistic effect of fluorine and nitrogen co-doping, J Mater Chem A 6 (2018) 13062–13074.

[11] B. Ou, J. Wang, Y. Wu, S. Zhao, Z. Wang, Efficient removal of Cr (VI) by magnetic and recyclable calcined CoFe-LDH/g-C_3N_4 via the synergy of adsorption and photocatalysis under visible light, Chem. Eng. J. 380 (2020) 122600.

[12] Y. Tian, L. Huang, X. Zhou, C. Wu, Electroreduction of hexavalent chromium using a polypyrrole-modified electrode under potentiostatic and potentiodynamic conditions, J. Hazard. Mater. 225-226 (2012) 15–20.

[13] Y. Wu, R. Wu, H. Zhou, G. Zeng, C. Kuang, C. Li, Sustainable electro-Fenton simultaneous reduction of Cr (VI) and degradation of organic pollutants via dual-site porous carbon cathode driving uncoordinated molybdenum sites conversion, Water Res. 259 (2024) 121835.

[14] A. Ihsanullah, A.M. Abbas, T. Al-Amer, M.J. Laoui, M.S. Al-Marri, M. Nasser, M. A. Khraisheh, Atieh, heavy metal removal from aqueous solution by advanced carbon nanotubes: critical review of adsorption applications, Sep. Purif. Technol. 157 (2016) 141–161.

[15] X. Ren, C. Chen, M. Nagatsu, X. Wang, Carbon nanotubes as adsorbents in environmental pollution management: a review, Chem. Eng. J. 170 (2011) 395–410.

[16] T.O. Ajiboye, O.A. Oyewo, D.C. Onwudiwe, Simultaneous removal of organics and heavy metals from industrial wastewater: a review, Chemosphere 262 (2021) 128379.

[17] C. Chen, P. Liu, Y. Li, H. Tian, Y. Zhang, X. Zheng, R. Liu, M. Zhao, X. Huang, Electro-peroxone enables efficient Cr removal and recovery from Cr(III) complexes and inhibits intermediate Cr(VI) generation in wastewater: performance and mechanism, Water Res. 218 (2022) 118502.

[18] H. Liu, G. Tian, W. Wang, J. Zhang, T. Wu, X. Ni, Y.-H. Wu, Carbon fiber-based flow-through electrode system (FES) for Cr(VI) removal at near neutral pHs via Cr (VI) reduction and in-situ adsorption of Cr (III) precipitates, Chem. Eng. J. 420 (2021) 127622.

[19] M. Li, K. Zuo, S. Liang, K. Xiao, P. Liang, X. Wang, X. Huang, Electrically tuning ultrafiltration behavior for efficient water purification, Environ. Sci. Technol. 54 (2020) 11536–11545.

[20] N. Chen, X. Cui, X. Sun, X. Yang, W. Yang, N. Ren, Y. Feng, Y. Tian, W. He, Advanced Cr(VI) removal from wastewater using migrating electric field-assisted electrocoagulation combined with capacitive deionization technology, J Water Process Eng 63 (2024) 105445.

[21] L. Yang, X. Liu, T. Yang, Z. Chen, J. Guo, L. Zheng, X. Xiao, G. Zeng, X. Luo, S. Luo, Electrochemical recovery of total Cr by reduction alongside immobilization using an acethydrazide functionalized Fe/Ni-MIL-53 MOF electrode, Resour. Conserv. Recycl. 191 (2023) 106884.

[22] Y. Wang, J. Zhang, W. Wang, T. Wu, Y. Sun, H. Wu, D. Chen, H. Liu, Enhancement of Cr(VI) reduction by polyaniline nanorod-modified cathode in flow-through electrode system, Chem. Eng. J. 429 (2022) 132553.

[23] D. Wang, J. Zhou, Y. Zhang, J. Zhang, J. Liang, J. Zhang, J. Li, The electrosorption of uranium (VI) onto the modified porous biocarbon with ammonia low-temperature plasma: kinetics and mechanism, Chem. Eng. J. 463 (2023) 142413.

[24] M.N. Kleinberg, C. Thamaraiselvan, C.D. Powell, A. Ronen, C.J. Arnusch, Reduction of Cr(VI) to Cr(III) by activated carbon cloth through adsorption and electrochemical processes, ACS Appl. Eng. Mater. 1 (2023) 901–912.

[25] Y.-U. Shin, W. Pan, S.K. Patel, J. Lim, L.R. Winter, W. Ma, S. Hong, M. Elimelech, Electrochemical chromium removal using nanodiamond enhanced flow-through electrosorption, Chem. Eng. J. 474 (2023) 145756.

[26] R. Patil, D. Jiang, X. Xu, N. Kumar, S. Bhattacharjee, S.K. Yadav, D. Kalyanasundaram, R.R. Salunkhe, A. Bhaumik, N. Khaorapapong, Y. Yamauchi, S. Dutta, Graphene-sponges containing multi-walled carbon nanotubes for electrosorption of salt-ions, Chem. Eng. J. 506 (2025) 159270.

[27] Y.-J. Lin, C.-C. Chen, Modeling salt adsorption in electrical double layer for capacitive deionization, AICHE J. 69 (2023) e18018.

[28] C. Rosales-Landeros, C.E. Barrera-Díaz, B. Bilyeu, V.V. Guerrero, F.U. Núñez, A review on Cr(VI) adsorption using inorganic materials, Am. J. Anal. Chem. 04 (2013) 8–16.

[29] B. Jiang, Q. Niu, C. Li, N. Oturan, M.A. Oturan, Outstanding performance of electro-Fenton process for efficient decontamination of Cr(III) complexes via alkaline precipitation with no accumulation of Cr(VI): important roles of iron species, Appl. Catal. B Environ. 272 (2020) 119002.

[30] Y.-J. Shih, Z.-S. Chen, C.-L. Chen, Y.-H. Huang, C.-P. Huang, Enhancing arsenic (III) removal by integrated electrocatalytic oxidation and electrosorption reactions on nano-textured bimetal composite of iron oxyhydroxide and manganese dioxide polymorphs (α-, γ-, β-, and ε-$Mn_xFe_{1-x}O$), Appl. Catal. B Environ. Energy 317 (2022) 121757.

[31] C.M. Stern, T.O. Jegede, V.A. Hulse, N. Elgrishi, Electrochemical reduction of Cr (VI) in water: lessons learned from fundamental studies and applications, Chem. Soc. Rev. 50 (2021) 1642–1667.

[32] J. Zhou, Y. Zhang, M. Balda, V. Presser, F.-D. Kopinke, A. Georgi, Electro-assisted removal of polar and ionic organic compounds from water using activated carbon felts, Chem. Eng. J. 433 (2022) 133544.

[33] W. Ma, S.K. Patel, M. Marcos-Hernandez, X. Wang, X. Zhou, W. Pan, Y. Shin, D. Villagran, M. Elimelech, Rapid, selective, and chemical-free removal of dissolved silica from water via Electrosorption: feasibility and mechanisms, Environ. Sci. Technol. 58 (2023) 947–959.

[34] I. Hakizimana, X. Zhao, C. Wang, E. Mutabazi, C. Zhang, Insights into the flow-through electrochemical system in water and wastewater treatment: influential factors, advantages, challenges, and perspective, Sep. Purif. Technol. 331 (2024) 125533.

[35] M. Pan, C. Shan, X. Zhang, Y. Zhang, C. Zhu, G. Gao, B. Pan, Environmentally friendly in situ regeneration of graphene aerogel as a model conductive adsorbent, Environ. Sci. Technol. 52 (2018) 739–746.

[36] M. Jiang, J. Huang, G. Yang, H. Wang, H.-F. Wang, F. Peng, Y. Cao, H. Yu, In-situ regeneration of carbon monoliths as an environmental-benign adsorbent for environmental remediation via a flow-through model, Sep. Purif. Technol. 314 (2023) 123542.

[37] S. Chen, K. Huang, H.-F. Wang, H. Wang, H. Yu, J. Huang, Y. Cao, Electric-field enhanced three-dimensional flexible carbon felt as a host for Pt^{4+} ions extraction, Chem. Eng. J. 490 (2024) 151835.

[38] Y. Wang, J. Xu, H. Liu, Y. Lu, D. Chen, G. Lu, Square-wave alternating voltage for enhancing Cr(VI) reduction in a carbon Fiber-based flow-through electrode system, ACS ES&T Eng. 2 (2022) 831–841.

[39] X. Yu, L. Zhang, M. Liang, W. Sun, pH-dependent sulfonamides adsorption by carbon nanotubes with different surface oxygen contents, Chem. Eng. J. 279 (2015) 363–371.

[40] Y. Song, J. Xie, Y. Song, H. Shu, G. Zhao, X. Lv, W. Xie, Calculation of standard electrode potential of half reaction for benzoquinone and hydroquinone, Spectrochim. Acta, Part A 65 (2006) 333–339.

[41] L.-S. Zhong, J.-S. Hu, H.-P. Liang, A.-M. Cao, W.-G. Song, L.-J. Wan, Self-assembled 3D flowerlike Iron oxide nanostructures and their application in water treatment, Adv. Mater. 18 (2006) 2426–2431.

[42] L.C. Hsu, S.L. Wang, Y.C. Lin, M.K. Wang, P.N. Chiang, J.C. Liu, W.H. Kuan, C. C. Chen, Y.M. Tzou, Cr(VI) removal on fungal biomass of Neurospora crassa: the importance of dissolved organic carbons derived from the biomass to Cr(VI) reduction, Environ. Sci. Technol. 44 (2010) 6202–6208.

[43] Y. Wang, G. Wen, Z. Liu, T.T. Thuy Nga, C.-L. Dong, J. You, C. Xie, S. Du, F. Zhang, Q. Liu, J. Wei, Y. Cao, X. Peng, Y. Yuan, Y. Wang, S. Wang, Bipolar electrochemical uranium extraction from seawater with ultra-low cell voltage, Nature Sustain. 8 (2025) 682–691.

[44] M. Mao, T. Yan, J. Shen, J. Zhang, D. Zhang, Capacitive removal of heavy metal ions from wastewater via an electro-adsorption and electro-reaction coupling process, Environ. Sci. Technol. 55 (2021) 3333–3340.
[45] Z. Yang, Y. Liu, R. Yang, B. Shi, P. Liu, L. Yang, A. Zhang, Z. Liu, T. Zhang, X. Li, Z. Li, Development and application of metal–organic frameworks and spherical carbon particles for efficient recovery of phenols and oils from coal chemical wastewater: a new full-process adsorption treatment mode, Chem. Eng. J. 498 (2024) 155219.
[46] F. Yao, M. Jia, Q. Yang, K. Luo, F. Chen, Y. Zhong, L. He, Z. Pi, K. Hou, D. Wang, X. Li, Electrochemical Cr(VI) removal from aqueous media using titanium as anode: simultaneous indirect electrochemical reduction of Cr(VI) and in-situ precipitation of Cr(III), Chemosphere 260 (2020) 127537.
[47] F. Rodriguez-Valadez, C. Ortiz-Exiga, J.G. Ibanez, A. Alatorre-Ordaz, S. Gutierrez-Granados, Electroreduction of Cr(VI) to Cr(III) on reticulated vitreous carbon electrodes in a parallel-plate reactor with recirculation, Environ. Sci. Technol. 39 (2005) 1875–1879.
[48] G. Almaguer-Busso, G. Velasco-Martínez, G. Carreño-Aguilera, S. Gutiérrez-Granados, E. Torres-Reyes, A. Alatorre-Ordaz, A comparative study of global hexavalent chromium removal by chemical and electrochemical processes, Electrochem. Commun. 11 (2009) 1097–1100.
[49] L.A.M. Ruotolo, J.C. Gubulin, Optimization of Cr(VI) electroreduction from synthetic industrial wastewater using reticulated vitreous carbon electrodes modified with conducting polymers, Chem. Eng. J. 149 (2009) 334–339.
[50] S.J. Kim, D.J. Ha, T.S. Koo, Simultaneous quantification of methylene blue and its major metabolite, azure B, in plasma by LC-MS/MS and its application for a pharmacokinetic study, Biomed. Chromatogr. 28 (2013) 518–524.
[51] M.A. Rauf, M.A. Meetani, A. Khaleel, A. Ahmed, Photocatalytic degradation of methylene blue using a mixed catalyst and product analysis by LC/MS, Chem. Eng. J. 157 (2010) 373–378.
[52] W. Ma, Z. Cheng, Z. Gao, R. Wang, B. Wang, Q. Sun, Study of hydrogen gas production coupled with phenol electrochemical oxidation degradation at different stages, Chem. Eng. J. 241 (2014) 167–174.
[53] S. Meshram, R. Limaye, S. Ghodke, S. Nigam, S. Sonawane, R. Chikate, Continuous flow photocatalytic reactor using ZnO–bentonite nanocomposite for degradation of phenol, Chem. Eng. J. 172 (2011) 1008–1015.